Journal of The Electrochemical Society

The Electrochemical Society
Advancing solid state & electrochemical science & technology

OPEN ACCESS

Fabrication of Plasmonic Optical Nanopore Platform for Single Molecule Sensing

To cite this article: Seong Soo Choi *et al* 2020 *J. Electrochem. Soc.* **167** 027503

Journal of the Electrochemical Society, 2020 **167** 027503

Fabrication of Plasmonic Optical Nanopore Platform for Single Molecule Sensing

Seong Soo Choi,[1,z] Sae-Joong Oh,[1] Yong Min Lee,[1] Hyun Tae Kim,[2] Soo Bong Choi,[2] and Byung Seong Bae[3]

[1]*Research Center for NanoBio Science, SunMoon University, Ahsan, Chungnam 31460, Republic of Korea*
[2]*Department of Physics, Incheon National University, Incheon 22012, Republic of Korea*
[3]*School of Electronics and Display Engineering, Hoseo University, Asan City, Chungnam 31499, Republic of Korea*

Recently there have been significant interests about fabrication of optical nanopore with its diameter range of 5 nm to 10 nm for single molecule analysis and manipulation. However, due to very small amount of the optical intensity through the tiny size of the nano-aperture much smaller than the optical wavelength, the optical intensity enhancement via plasmonic effect by using pore array or periodic groove patterns have been tried. Also, the double slits with nanoscale width are reported to provide the constructive periodic modulation for the transverse-magnetic (TM) wave mode. In this report, the nanoscale double slit with an Au aperture array have been fabricated and optically characterized.

 [DOI: 10.1149/1945-7111/ab615e]

Manuscript submitted September 18, 2019; revised manuscript received December 8, 2019. Published January 2, 2020.

About 60 years ago, the biological cell counter with an electrical detection technique was invented by Dr. Coulter. Due to fast developing nanofabrication technology, the smaller nanobio device for single molecule detection has been tested and manufactured.[1] The fabricated portable nanopore device with an electrical detection technique by using a focused electron beam technique was reported to provide the huge errors,[2,3] however, sequencing accuracy with over 95 percent is recently reported.[4] Various fabrication techniques; physical drilling either by using a focused ion beam technique, or by a focused electron beam technique for a single nanometer size pore, and a controlled dielectric breakdown technique for relatively large nanopore of a ~40 nm dimeter are well documented.[5,6] Microfabrication of nanopore for an electrical detection technique has been also reported using Si chemical etching techniques.[7,8] The electrical detection method of the secretome and the transfection of a single cell via a solid-state nanopore is well documented.[9]

However, considering the fact that most biosensors are utilizing the optical detection technique, the optical pore device can be an excellent candidate for the next generation single molecule sensor. The tiny nano-aperture with its diameter of ~10 nm or less would have negligible optical transmission from Bethe's law; $T \sim (d/\lambda)^4$. Optical transmission through the tiny nano-aperture should be enhanced either by providing the groove patterns or periodic arrays.[10] The nanopore with ~ nm diameter for an optical detection technique has yet to be fabricated.

The enhancement of light transmission through a nano-aperture surrounded by periodic patterns on the input side of a flat plane has been also reported,[10] and a directional beaming effect through an aperture with a periodic pattern on the exit side of a flat membrane has been also reported.[11] We previously reported fabrication of the nano-aperture surrounded by the periodic patterns on the outside of the pyramidal probes to improve the low transmittance of light through the nanosize aperture.[12–14] Huge optical intensity enhancement of $\sim 10^3$-fold increase through a pyramidal aperture has been reported for the groove patterns whose pitch matched the surface plasmon wavelength, which can be attributed to the coupling of a backward diffracted surface wave with the patterned grooves on the exit side of the pyramid. Even without a nano-aperture on top of the an elliptically patterned pyramid, a huge 10^3-fold increase is also reported in the transmitted optical power due to the strong coupling of the surface plasmonic modes with the photonic modes of the input beams.

We have also fabricated the optical nanopore with its diameter ranging from 10 nm to 3 nm on the on the flat Au thin membrane by using various surface modifications.[15–20] Au-aperture with its diameter ranging from 50 nm to 100 nm was initially drilled by 30 keV Ga focused ion beam technique (FIB), then by using various electron beam irradiations such as field emission electron beam microscopy (FESEM) and transmission electron beam microscopy (TEM), a nanopore with its diameter of 5 nm was formed on the diffused membrane inside the FIB-drilled Au aperture. Optical intensity measurements did not reveal any differences between through the nano-aperture without a diffused Au–C membrane, and through the nano-aperture with a diffused membrane. This can be attributed to the diffused membrane thickness below the Au skin depth ($\ll$20 nm), and low Au atomic concentration ($\ll$50%) on the membrane.[14,18]

Classical double slits with micron size slit width would provide the far field interference patterns, regardless of the polarization states. However, for the nanoscale double slits, the surface plasmonic wave from the nanoscale slits can provide the periodic interference phenomena for the TM wave between the nanoscale slits, which reduces or enhances the intensity of the far-field.[21–23] When the incident light is TM-polarized, electric field aligned perpendicular to the slits, the surface plasmon wave that is excited at one of the slits propagates towards its other slit. For the case of TM polarization, the transmission via slits is seen to be sinusoidally modulated as a function of wave number, and the modulation period becomes inversely proportional to the slit separation. For a TE (transverse electric)-polarized incident beam there will be no modulation. There will be three possible types of physical mechanisms; first, the slits transmit part of the incident radiation, together giving rise to a conventional Young-type interference pattern. Second, each slit scatters part of the incident radiation into a plasmonic channel, bridging the momentum gap between the surface plasmon and free-space radiation. Third, each slit provides a mechanism for back-converting a surface plasmon into free-space radiation. Hence, the strength of each of these sources is enhanced or reduced due to the interference of a photonic and a plasmonic channel. With proper controlling the pitch of the aperture and the nanoscale slits separation gap, the enhanced optical intensity would be obtained. In this report, fabrication of the nano-pore platform which consists of Au nano-aperture array sidelined with the nanoscale double slits will be presented.

Experimental

Fabrication of plasmonic nanopore platform and its optical characterization.—Initially, the ~200 nm Au thin films were

[z]E-mail: sscphy2010@gmail.com

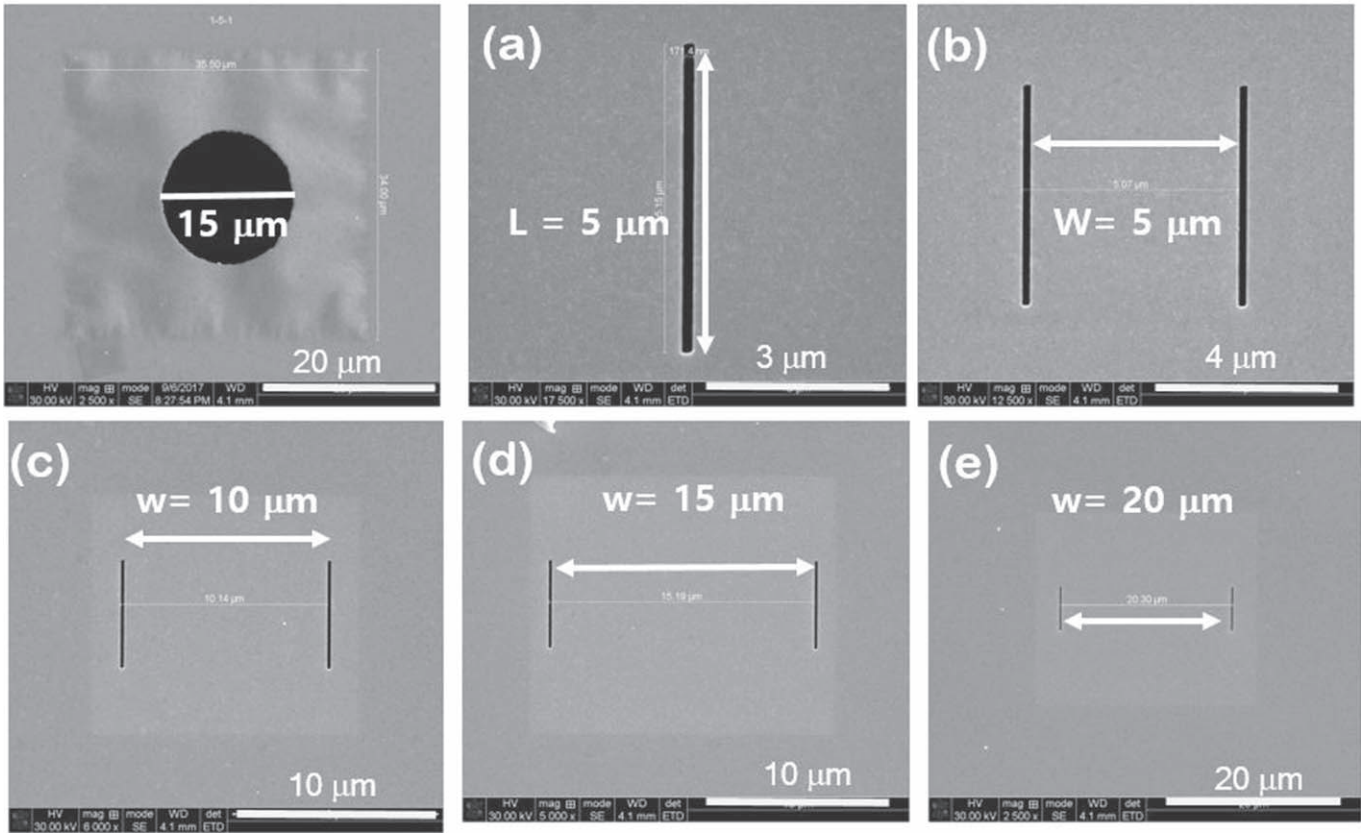

Figure 1. The FESEM images present a circular hole with a 15 mm diameter as a calibration control sample for the optical characterization (top left), and the 5 μm long single slit (a), double slits with a 5 μm separation (b), a 10 μm separation (c), a 15 μm separation (d), and a 20 μm separation (e).

deposited on the 5 nm thick SiN commercial TEM grids (www.temwindows.com), followed by dry etching of supporting the SiN membrane. Then, drilling for Au aperture array with its diameter of ~200 nm was followed by using focused Ga ion beam technique (Dual beam Helios, FEI). The nanoscale slits with (~170 nm wide and ~5 mm long) size were drilled, and electron beam irradiations were carried out by using as transmission electron microscopy (TEM) (JEM-2010, JEM-2100F and JEM-3011HR) and field emission scanning electron microscopy (FESEM, JSM 6400) were utilized. TEM can provide high electron voltages ranging from 100 keV to 300 keV and the currents with ~ order of 100 pA, while FESEM (Dual Beam Helios, FEI) will provide the probe current of 1.4 nA nm^{-2} ranging from 2 keV to 20 keV. Then, its optical characterization was carried out. by using a white light using Halogen lamp installed at Nikon TE eclipse microscope with a spectrometer (SpectraPro 2300i (150 g mm^{-1}), Princeton Instruments).

***Experimental results.*—**Figure 1 presents the large circular aperture with a 15 μm diameter for a calibration of the optical beam (top left), and a single slit with a (~170 nm wide x ~5 μm long) (a). Double slits with double slits with 5 μm separation (b), 10 μm separation (c), 15 μm separation (d), and 20 μm separation are presented (e). Figure 2 presents TEM images of the 5 μm long slit, and diffused Au particles due to the thermal spike effect during

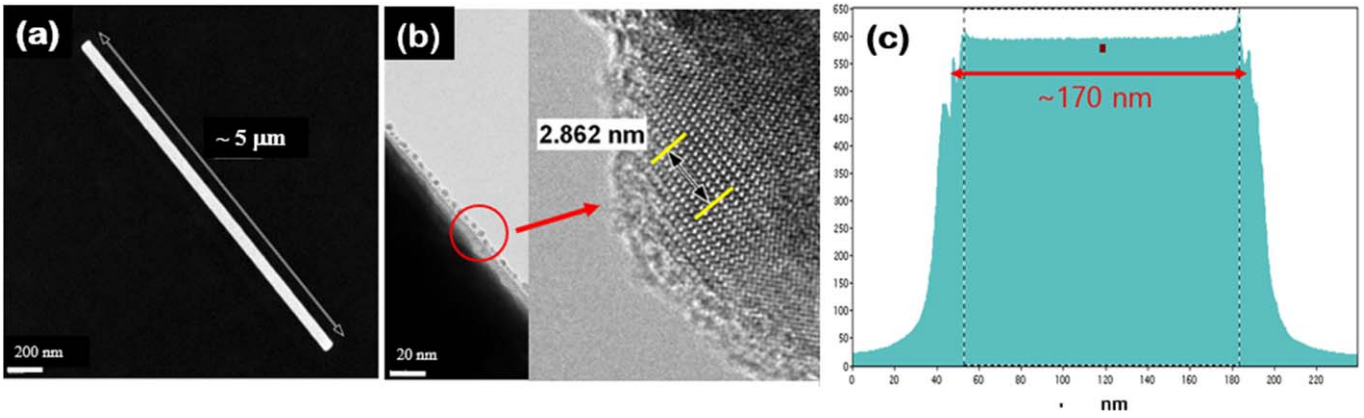

Figure 2. TEM images show a ~5 μm long single slit (a), the Au nanoparticles formed and diffused on the slit edge due to high temperature effect from the thermal spike during the FIB drilling procedure (b), and an Au nanoparticle with a 2.862 nm width for 10 atomic spacing is presented. An electron beam profile through the ~170 nm wide gap of the slit on the electron beam detector is also shown (c).

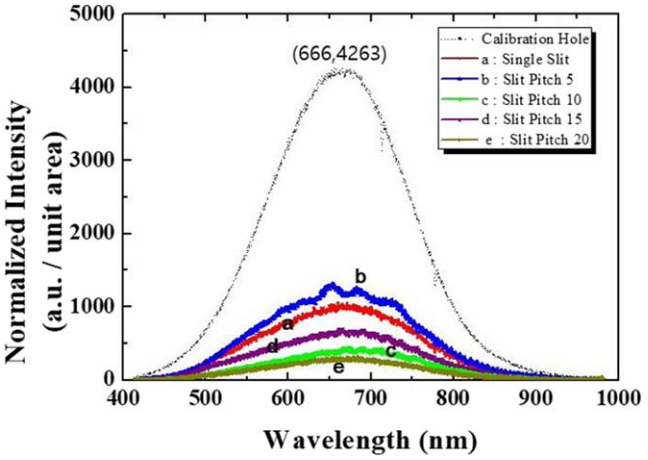

Figure 3. These graphs present the normalized optical intensities to slit open gap area through the double nanoscale slits for different pitches (separations) versus input wavelength. The dashed line indicates the free space input intensity with its peak point (666, 4263). Red a line and blue b line present the output intensities for single slit and double slit with a 5 μm pitch. Green c line, violet d line, and dark yellow e line indicate the output intensities from double slits with pitches of 10 μm, 15 μm, and 20 μm, respectively.

the FIB drilling procedure presented in Fig. 2(b). And the electron beam profile at the electron beam detector through the slit with a $\sim$ 170 nm width is presented in Fig. 2(c).

We investigated the transmitted optical intensities dependent upon the pitches (separations) of the nanoscale slits. Figure 3 presents the normalized optical peak intensities versus wavelength for the slits with different pitches. The red line (a) and the blue line (b) display the optical intensities for the single slit and for the slits with a 5 μm pitch, respectively. And the green line (c), the violet line (d), and the dark yellow (e) line indicate the normalized peak optical intensities for the slits with the 10 μm pitch, the 15 μm pitch, and the 20 μm pitch, respectively. The optical intensities for (c), (d) and (e) are weaker than those for the single slit (a), and also for the double slits with a 5 μm pitch (b). However, for the 15 μm pitch, the optical intensity in (c) is measured to be greater than those for 10 μm pitch (c). Then, for the 20 μm pitch (e), the optical intensity is measured to be much weaker than those for 10 μm pitch. These optical intensity variations dependent upon the increased slit pitch indicate the constructive interferences for the slits with a 5 μm pitch, and a 15 μm pitch. The periodical interference phenomena dependent upon the pitch is also presented in Table I. The optical intensity ratio is defined as the total integrated output intensity for the entire optical wavelength divided by the total input intensity (free space intensity). With increasing the separation of the slits from 5 μm to 20 μm, the decreased interference optical intensity is clearly shown. However, the optical ratio (0.1694) from the sample with 15 μm separation is higher than that (0.1004) with 10 μm separation. This could be attributed from periodic modulation effect dependent upon the slit separation.

Figure 4 presents the (7 $\times$ 7) Au aperture arrays on the 200 nm Au deposited film with its pitches of 530 nm in (a), 780 nm in (b), and 1064 nm in (c). The aperture diameters are set to be $\sim$200 nm. And after the optical characterization, the nanoscale double slits were drilled, the width and the length of the drilled nanoscale slit are measured to be $\sim$170 nm wide and $\sim$5 μm long, respectively.

Figure 5 presents the optical enhancement factor versus input wavelength. The optical enhancement factor is defined as the ratio of the free space input intensity to the output intensity. Highest enhancement factor of 1.73 at 713 nm is presented for (7 $\times$ 7) array with a 530 nm pitch, and the enhancement factors of less than 0.5 from the entire wavelength ranging from 550 nm to 800 nm are shown for the (7 $\times$ 7) array with 780 nm pitch and 1060 nm pitch in Fig. 5(a). Figure 5(b) presents the enhancement factor of 8.36 at 719 peak for the (7 $\times$ 7) array with 530 nm pitch, and the enhancement factor less than 2 for the entire wavelength regime ranging from 550 nm to 800 nm. The enhancement increase at the peak from 1.72 to 8.36 can be attributed to the nanoscale slits effect from additional constructive interferences between the surface plasmonic wave arising from the slits and the surface plasmon wave from the (7 $\times$ 7) aperture array.

Results and Discussion

We have fabricated the nanopore platform with nano-aperture array and nanoscale double slits dependent upon the pitch between two slits. For nanoscale double slits without a nano-aperture array, at 5 μm pitch and 15 μm pitch, the optical intensities are measured to be greater than that for a single slit, due to the constructive interference of the surface plasmon wave from the slits. At 10 μm pitch and 20 μm pitch, the optical intensities are found to be weaker than that even for the single slit due to destructive interference from the slits. These observations are agreeable with previous experiments by others.

For the (7 $\times$ 7) nano-aperture array without nanoscale double slits, the highest optical enhancement factor of 1.73 at the 713 nm peak position is presented for the (7 $\times$ 7) array with a 530 nm aperture-pitch, among the nano-aperture array with aperture-pitches of 530 nm, 780 nm, and 1060 nm. For the aperture array sidelined with nanoscale double slits, the enhancement factor of 8.36 at 719 peak for the (7 $\times$ 7) array with a 530 nm aperture-pitch is observed. The huge enhancement factor increase at the peak position from 1.72 to 8.36 can be attributed to the constructive interferences from the nanoscale double slits, in addition to the surface plasmon resonances among the nano-aperture array.

Conclusions

We have fabricated the nano-aperture array with nanoscale double slits, in addition to the nanoscale double slits. For nanoscale double slits, we observed the highest optical intensity at slits

Table I. Please note that the normalized optical intensities for 10 μm pitch, 15 μm pitch and 20 μm pitch are measured to be lower than that of a single slit. In addition, the normalized optical intensity (0.3149) for 5 μm pitch is greater than those for a single slit, and 10 μm pitch, 15 μm pitch and 20 μm pitch. Furthermore, the optical intensities for 5 μm pitch and 10 μm pitch become reduced from 0.3149 to 0.1004, then become increased from 0.1004 to 0.1694. The optical intensities seem to oscillate periodically as the pitches become greater.

Sample name	Pitch	Total area (μm^2)	Integrated intensity	Ratio(I_{out}/I_{free})
21-20-2	Calibration hole	185.78	886,847.2	1.0000
6-10-1-A	Single slit	0.87	227,171.8	0.2562
6-10-1-C	5.07 μm	1.75	279,288.9	0.3149
6-10-1-E	10.14 μm	1.75	88,999.0	0.1004
6-10-1-G	15.19 μm	1.75	150,213.9	0.1694
6-10-1-I	20.30 μm	1.75	62,952.3	0.0710

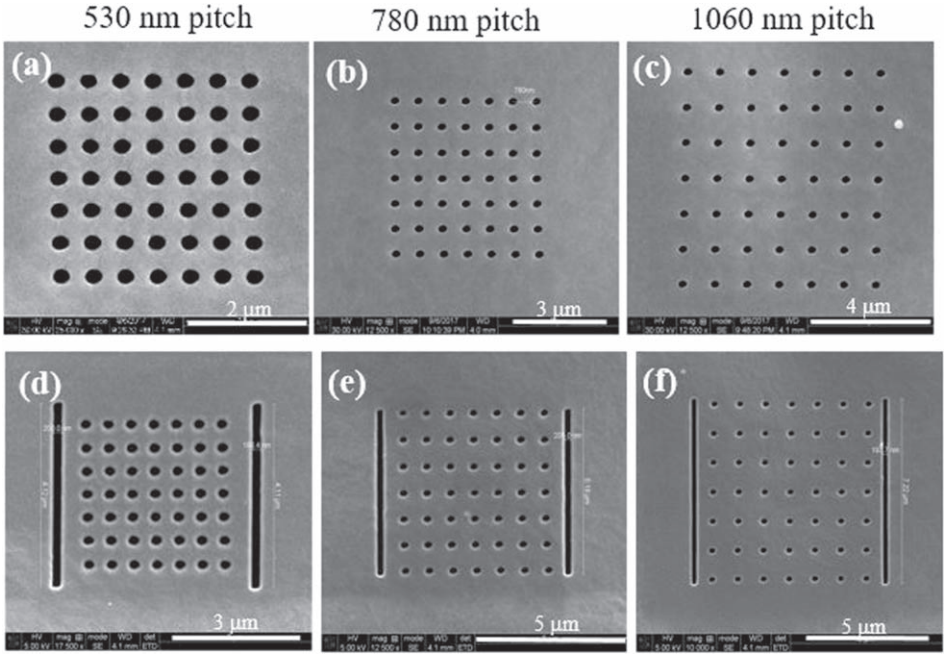

Figure 4. FESEM images present (7 × 7) arrays with its diameter of ∼200 nm, and also circular aperture arrays with pitches of 530 nm, 780 nm, and 1060 nm without nanoscale double slits (a–c), and with double slits (d–f).

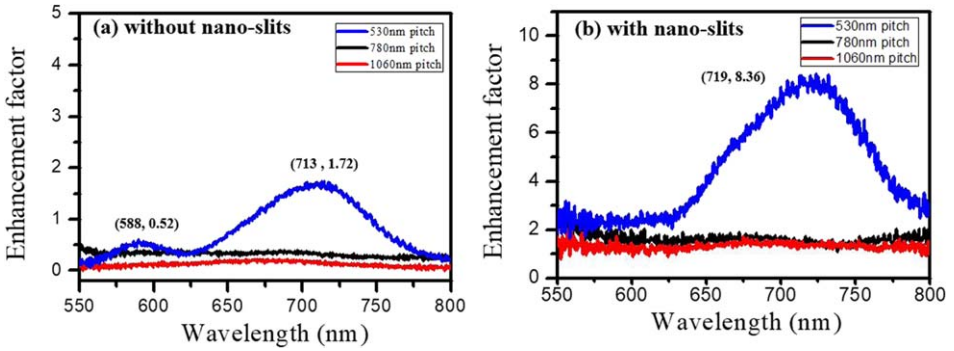

Figure 5. The enhancement factors versus input optical wavelength are presented for the (7 × 7) Au nano-aperture array without nanoscale double slit (left, a), and for (7 × 7) array with the slits (right, b). Highest enhancement factor of 1.73 at 713 is presented for (7 × 7) array without double slits for the 530 nm pitch, and the enhancement factor of 8.36 at 719 peak for the (7 × 7) array with double slits for the 530 nm pitch.

separations of 5 μm, and higher intensities at the 15 μm slit-pitch than others due to surface plasmonic interference. For nano-aperture (7 × 7) array with a 530 nm aperture -pitch sidelined with the nanoscale double slits, the highest enhancement factor of ∼8.4 at 719 nm peak position is obtained. The nanoscale aperture platform with huge optical enhancements can be utilized as a next generation bio sensor device.

Acknowledgments

This work was supported by the research funding programs (Development of Biofriendly Optical Nanopore, 2018R1D1A1B07 050106) under the Basic Science Research Program through the National Research Foundation (NRF) funded by the Ministry of Education, Science and Technology, South Korea.

References

1. M. Muthukumar, C. Plesa, and C. Dekker, *Phys. Today*, **68**, 40 (2015).
2. A. Mikheyev and M. M. Y. Tin, *Mol. Ecol. Resour.*, **14**, 1097 (2014).
3. E. C. Hayden, *Nature*, **521**, 15 (2015).
4. A. D. Tyler, L. Mataseje, C. J. Urfano, L. Schmidt, K. S. Antonation, M. R. Mulvey, and C. R. Corbett, *Sci. Rep.*, **8**, 10931 (2018).
5. A. J. Storm, J. H. Chen, X. S. Ling, H. W. Zandbergen, and C. Dekker, *Nat. Mater.*, **2**, 537 (2003).
6. I. Yanagi, R. Akahori, and K. Takeda, *Sci. Rep.*, **9**, 13143 (2019).
7. D. Ge, L. Lu, J. Zhang, L. Zhang, J. Ding, and P. J. Reece, *ECS J. Solid State Sci. Technol.*, **6**, 893 (2017).
8. Y. Wanga, Q. Chena, T. Dengb, and Z. Liua, *ECS J. Solid State Sci. Technol.*, **6**, 760 (2017).
9. V. Kurza, E. Nelsona, T. Tanakab, and G. Timpa, *ECS Trans.*, **64**, 15 (2014).
10. T. W. Ebbesen, H. J. Lezec, H. F. Ghaemi, T. Thio, and P. A. Wolff, *Nature*, **391**, 667 (1998).
11. H. J. Lezec, A. Degiron, E. Devaux, R. A. Linke, L. Martin-Moreno, F. J. Garcia-Vidal, and T. W. Ebbesen, *Science*, **297**, 820 (2002).
12. D. W. Kim, Y. C. Kim, O. Suwal, V. Jha, M. J. Park, and S. S. Choi, *Mater. Sci. Eng. B*, **149**, 242 (2008).
13. S. S. Choi, O. K. Suwal, V. Jha, D. W. Kim, and M. J. Park, *Curr. Appl Phys.*, **9**, S131 (2009).
14. S. S. Choi, M. J. Park, C. H. Han, Y. S. Kim, N. K. Park, S. H. Han, and H. Choo, *J. Vac. Sci. Technol. B*, **33**, 06F203 (2015).
15. S. S. Choi, M. G. Park, T. Yamaguchi, C. H. Han, S. J. Oh, K. J. Park, J. H. Yoo, Y. S. Kim, and N. K. Park, *ECS Trans.*, **75**, 281 (2016).
16. S. S. Choi, M. J. Park, C. H. Han, S. J. Oh, H. T. Kim, S. B. Choi, and Y. S. Kim, *ECS Trans.*, **85**, 69 (2018).
17. S. S. Choi, S. J. Oh, C. H. Han, N. K. Park, Y. S. Kim, J. H. Yoo, and K. J. Park, *Surf. Coating. Technol.*, **306**, 113 (2016).

18. S. S. Choi, M. J. Park, T. Yamaguchi, C. H. Han, S. J. Oh, S. I. Kim, K. J. Park, J. H. Yoo, Y. S. Kim, and N. K. Park, *Sens. Bio-Sens. Res.*, **7**, 153 (2016).
19. S. S. Choi, M. J. Park, T. Yamaguchi, S. I. Kim, K. J. Park, and N. K. Park, *Appl. Surf. Sci.*, **310**, 196 (2014).
20. S. S. Choi, S. J. Oh, C. H. Han, D. J. Park, S. B. Choi, Y. S. Kim, and N. K. Park, *J. Vac. Sci. Technol. B*, **35**, 04F107 (2017).
21. H. F. Schouten, N. Kuzmin, G. Dubois, T. D. Visser, G. Gbur, P. F. A. Alkemade, H. Blok, G. W.'t Hooft, D. Lenstra, and E. R. Eliel, *Phys. Rev. Lett.*, **94**, 053901 (2005).
22. C. H. Gan, G. Gbur, and T. D. Visser, *Phys. Rev. Lett.*, **98**, 043908 (2007).
23. M. Verma, S. Joshi, N. S. Bisht, H. C. Kandpal, P. Senthilkumaran, and J. Joseph, *J. Opt. Soc. Am.*, **29**, 195 (2012).